



1 Evaluation of Single- and Multiple-Doppler Lidar Techniques to Measure

2 Complex Flow during the XPIA Field Campaign

3 by

4 Aditya Choukulkar^{1,2*}, Alan Brewer², Scott P. Sandberg², Ann Weickmann^{1,2}, Timothy A.
5 Bonin^{1,2}, R. Michael Hardesty^{1,2}, Julie K. Lundquist^{3,4}, Ruben Delgado⁵, G. Valerio Iungo⁶, Ryan
6 Ashton⁶, Mithu Debnath⁶, Laura Bianco^{1,7}, James M. Wilczak⁷, Steven Oncley⁸, Daniel Wolfe⁷

⁷ *¹Cooperative Institute for Research in Environmental Sciences, Boulder CO*

²*Chemical Sciences Division, National Oceanic and Atmospheric Administration, Boulder CO*

⁹*³University of Colorado Boulder, CO*

10 *⁴National Renewable Energy Laboratory, Golden CO*

11 *⁵University of Maryland Baltimore County, MD*

12 *⁶University of Texas at Dallas, Richardson TX*

⁷Physical Sciences Division, National Oceanic and Atmospheric Administration, Boulder CO

⁸National Center for Atmospheric Research, Boulder CO

15

16

17 For Submission to: Atmospheric Measurement Techniques

18

19 Corresponding Author*: Aditya Choukulkar

20 Cooperative Institute for Research in Environmental Sciences
21 University of Colorado,
22 Boulder, CO 80305

23

24 Telephone: 303-497-4016

25 Email: aditya.choukulkar@noaa.gov

26 Fax: 303-497-5318

27

28



29 **Abstract:**

30 Accurate three-dimensional information of wind flow fields can be an important tool in
31 not only visualizing complex flow, but also understanding the underlying physical processes and
32 improving flow modeling. However, a thorough analysis of the measurement uncertainties is
33 required to properly interpret results. The XPIA (eXperimental Planetary boundary layer
34 Instrumentation Assessment) field campaign conducted at the Boulder Atmospheric Observatory
35 (BAO) in Erie, CO from 2 March – 31 May 2015 brought together a large suite of in-situ and
36 remote sensing measurement platforms to evaluate complex flow measurement strategies.

37 In this paper, measurement uncertainties for different single and multi-Doppler strategies
38 are investigated. The tradeoffs (such as time/space resolution vs. spatial coverage) among the
39 different measurement techniques are evaluated using co-located measurements made near the
40 BAO tower. Sensitivity of the single/multi Doppler measurement uncertainties to averaging
41 period are investigated using the sonic anemometers installed on the BAO tower as the standard
42 reference. Finally, the radiometer measurements are used to partition the measurement periods
43 as a function of atmospheric stability to determine their effect on measurement uncertainty.

44 It was found that with increase in spatial coverage and measurement complexity, the
45 uncertainty in the wind measurement also increased. For multi-Doppler techniques, the increase
46 in uncertainty for temporally uncoordinated measurements is possibly due to requiring additional
47 assumptions of stationarity and/or horizontal homogeneity. It was also found that wind speed
48 measurement uncertainty was lower during stable conditions compared to unstable conditions.

49

50

51

52

53

54

55



56 **1. Introduction**

57 Scanning coherent Doppler Light Detection and Ranging (LIDAR) systems have proved
58 to be invaluable tools for wind measurements in research as well as commercial applications. A
59 valuable advantage of scanning Doppler lidar systems is its ability to make measurements over
60 horizontal and vertical extents using a combination of azimuthal, Plan Position Indicator (PPI)
61 scans and vertical plane (RHI) scans. Doppler lidars measure the projection of the wind velocity
62 along the beam pointing direction denoted as line of sight (LOS) velocity or radial velocity given
63 in Eq. 1.

64
$$V_r = u \sin \varphi \cos \theta + v \cos \varphi \cos \theta + w \sin \theta \quad (1)$$

65 where, V_r is the LOS velocity, u , v , w are the velocity components in the east-west direction, the
66 north-south direction, and in the vertical respectively; θ and φ are the azimuth and elevation
67 angles respectively. In order to derive the 2-dimensional or 3-dimensional wind velocity
68 requires the use of suitable measurement strategies and/or velocity retrieval algorithms.

69 The 2-D and 3-D wind measurements from Doppler lidars are useful in various fields of
70 study such as boundary layer meteorology (Fernando et al., 2015; Vanderwende et al., 2015), air
71 quality (Barlow et al., 2011; Collier et al., 2005) wind energy research (Banta et al., 2015; Käslar
72 et al., 2010; Mikkelsen, 2014; Newsom et al., 2015) among others. The simplest techniques to
73 derive a profile of wind speed and direction using a single Doppler lidar are the Velocity
74 Azimuth Display (VAD) technique (Browning and Wexler, 1968) and the Doppler Beam
75 Swinging (DBS) technique (Strauch et al., 1984). These techniques assume horizontal
76 homogeneity of the wind in the measurement volume to estimate the profile of wind speed and
77 direction. Other techniques such as the Velocity Volume Processing (VVP) (Waldteufel and
78 Corbin, 1979) and the “Arc Scan” technique (Wang et al., 2015) limit the assumption of
79 horizontal homogeneity to smaller volumes within the lidar scans or to certain azimuth ranges
80 respectively, allowing to better preserve the spatial variability information at the expense of
81 increased uncertainty in the wind retrieval, especially when the wind direction is perpendicular to
82 the scan sector (Krishnamurthy et al., 2013).

83 A common method to make wind field measurements without assumption of spatial
84 homogeneity is through multi-Doppler techniques. “Virtual towers” (Calhoun et al., 2006) use



multiple Doppler lidars to interrogate a common volume in space in a temporally coordinated fashion, iterating through several height in order to create a wind profile. Several configurations of multi-Doppler scanning have been tested to quantify the skill in deriving two and three-dimensional wind fields. For example, co-planar RHI scans were used to study flows in mountain valleys (Hill et al., 2010) and within a meteor crater (Cherukuru et al., 2015), co-planar conical scans (PPIs) have been used to study coherent structures (Newsom et al., 2008; Träumner et al., 2015) and wind turbine wakes (Vollmer et al., 2015). Three-dimensional wind field measurements made using dual-Doppler intersecting RHI scans and using continuity to estimate the vertical velocity were used to study flow upstream and downstream of a utility scale wind turbine (Newsom et al., 2015). Three-dimensional wind and turbulence measurements using fully coordinated short-range continuous wave triple lidars (Mikkelsen et al., 2008) and long-range triple lidar scanning (Berg et al., 2015) have been demonstrated to provide high quality measurements of complex flow. In addition, manually coordinated triple lidar measurements (Wang et al., 2016) were also tested and showed promise in measuring the three-dimensional wind fields operationally. The Lower Atmospheric Boundary Layer Experiment (LABLE) validated wind and turbulence measurements from triple Doppler lidar measurements (Klein et al., 2015; Newman et al., 2016).

In addition to multi-Doppler approaches to measuring complex flow, several techniques enable wind field retrievals from single Doppler lidars which resolve the spatial variability measured by the lidar. For example, the Optimal Interpolation (OI) technique allows 2-D wind field retrievals on azimuthal scans (Choukulkar et al., 2012) without assumption of homogeneity of the wind field. In addition, variational methods can determine the wind fields from single or multiple Doppler lidars (Chan and Shao, 2007; Drechsel et al., 2009; Newsom et al., 2008).

The choice of the measurement strategy and the retrieval algorithms come with assumptions inherent to their process which need to be properly understood to interpret the measurements made. Several studies have been conducted to evaluate the measurement accuracy of the various single and multi-Doppler techniques. For example, measurement uncertainties in wind measurements made using the DBS technique in complex terrain were investigated by Bingöl et al., 2009 while Lundquist et al., 2015 studied the uncertainties in wind measurements using the DBS technique in presence of complex flow by simulating lidar



115 measurements within a wind turbine wake using a wind field created with large-eddy simulation.
116 Wind field measurements made using the virtual towers technique has been validated (Damian et
117 al., 2014; Gunter et al., 2015) to show high skill in measuring 2-D wind fields and (Stawiarski et
118 al., 2013) did a detailed error analysis of dual-Doppler co-planar PPI technique. Uncertainties in
119 three-dimensional wind field retrievals using triple Doppler lidar techniques have also been
120 investigated. For example, (Fuertes et al., 2014) and (Newman et al., 2016) presents a detailed
121 analysis of 3-D winds and turbulence measurements made using staring triple Doppler
122 measurements, while (Berg et al., 2015) present validation of three-dimensional wind
123 measurements made through continuous scanning.

124 While considerable effort has been devoted to evaluating each of these wind
125 measurement techniques, few studies have inter-compared wind measurements from multiple
126 Doppler lidar techniques against a common standard or discussed the trade-offs between the
127 different measurement techniques. The eXperimental Planetary boundary layer Instrumentation
128 Assessment (XPIA) field campaign conducted at the Boulder Atmospheric Observatory (BAO)
129 in Erie, CO from 2 March – 31 May, 2015 provided an unique opportunity to inter-compare (in
130 similar atmospheric conditions) various single and multi-Doppler wind measurement strategies
131 to measure complex flow. In this paper, precision of single and multiple Doppler lidar
132 techniques to measure complex flow are evaluated. In addition, the trade-offs in terms of
133 measurement precision, spatial coverage and temporal resolution between the various
134 measurement techniques are also discussed. The paper is organized as follows: the experiment
135 setup and measurement area is described in Section 2. Section 3 presents analysis of the LOS
136 velocity uncertainty and Section 4 presents results from the validation of the different
137 measurement techniques tested in XPIA. This is followed by a discussion of the results in
138 Section 5. Concluding remarks are presented in Section 6.

139 **2. Experiment Setup**

140 The XPIA field study, funded by the U.S. Department of Energy (DOE) within the
141 Atmosphere to electrons (A2e) program, had the goal to assess current capabilities for measuring
142 complex flow in and near wind farms using remote sensing instrumentation. With this goal in
143 mind, a large suite of instrumentation was deployed near the BAO (Kaimal and Gaynor, 1983)
144 facility in Erie, CO. The instrumentation included six scanning Doppler lidars (four capable of



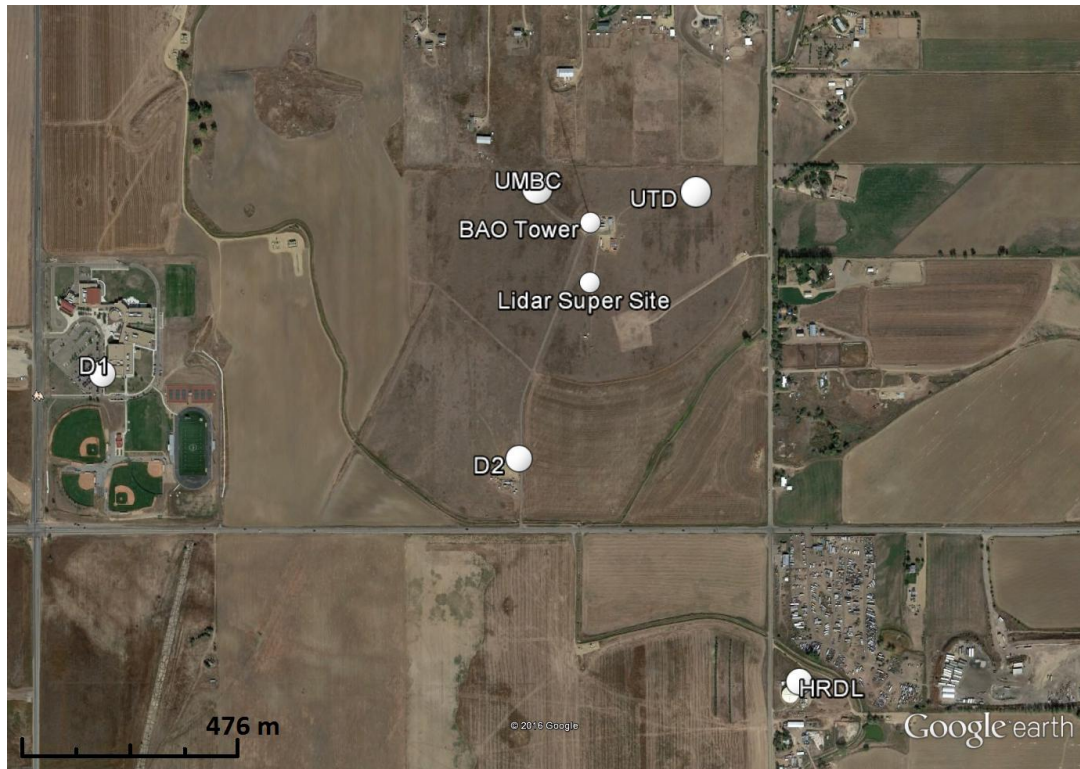
145 coordinated scanning) and five vertically-profiling lidars. Lundquist et al. (2016) gives a
146 detailed description of the XPIA field study along with an overview of the instrumentation
147 deployment. Herein for sake of brevity, only the details of the scanning lidar deployment used
148 for testing the various single and multi-Doppler measurements are described. These lidars
149 included two Leosphere 200S® scanning lidars (named “D1” and “D2”) and the High Resolution
150 Doppler Lidar (HRDL) from the National Oceanic and Atmospheric Administration (NOAA),
151 one Leosphere 200S® scanning Doppler lidar from the University of Texas at Dallas (“UTD”)
152 and one Leosphere 200S® from the University of Maryland Baltimore County (“UMBC”).
153 Figure 1 shows the deployment locations of these scanning lidars with respect to the 300-m tall
154 instrumented BAO tower. The pulse-width and time accumulation for each of the lidars used in
155 the analysis presented in this paper is given in Table 1. All the wind measurement comparisons
156 presented in this paper are with respect to the measurements made by the south-east sonic
157 anemometers installed on the BAO tower as the center of the lidar measurement volume (and the
158 range-gates) were always south of the BAO tower. The sonic anemometer data are filtered to
159 remove tower wake effects using the criteria defined in McCaffrey et al. (2016).

160 Table 1. Lidar operational parameters

Lidar	Pulse Width (m)	Time Accumulation (s)
HRDL	30	0.5
D1	50	0.5
D2	50	0.5
UTD	50	0.5
UMBC	50	1 ¹

161

¹ Longer accumulation time was selected to ensure sufficient range



162

163 Figure 1. Scanning Doppler lidar deployment location during the XPIA field campaign.

164

165 During the initial stages of the experiment, all the scanning Doppler lidars described
166 above were tested for scanner pointing accuracy. For lidars involved in coordinated scanning
167 (D1, D2 and UTD), the repeatability as well as accuracy of pointing and reproducibility of time
168 synchronization were tested. The details of these tests and the results are described in detail by
169 (Lundquist et al. 2016b) and summarized in Table 2. The scan initialization delay estimates
170 from time synchronization tests for the lidars involved in coordinated scanning are summarized
171 in Table 3. The scan initialization delay is defined as the time delay between the desired scan
172 start time and the actual scan start time. In addition to the scan initialization delay, the delay
173 introduced due to each of the lidars scanning varying range of azimuths to reach the
174 measurement location was characterized and accounted for during the scan strategy design for
175 each of the measurement techniques evaluated. The net impact of all the pointing and time
176 synchronization uncertainties is that all the systems could make measurements at a prescribed



177 location at a given time with pointing uncertainty of less than 0.15° and time uncertainty of less
178 than 0.4 s.

179 Table 2. Scanner pointing accuracy and repeatability estimates for the scanning Doppler lidars

Lidar	Pointing Error (°)	Repeatability in AZ (°)	Repeatability in EL (°)
HRDL	< 0.1	~0.05	~0.05
D1	~ 0.15	0.01	0.05
D2	~ 0.15	0.01	0.05
UTD	~ 0.15	Not Determined	Not Determined
UMBC	~ 0.15	Not Determined	Not Determined

180

181 Table 3. Scan initialization delay estimates for the scanning Doppler lidars

Lidar	Scan Initialization Delay (s)	Std Deviation of the Delay (s)
HRDL	43.28 ²	0.42
D1	3.98	0.29
D2	3.81	0.3
UTD	0.79	0.3
UMBC	Not Applicable ³	Not Applicable

182

183 In this paper, the following Doppler lidar measurement techniques will be discussed:

184 1. Virtual tower stares
185 2. Coordinated triple lidar sparse sampling scans
186 3. Uncoordinated multi-Doppler volume scan
187 4. Single Doppler lidar wind retrieval using the Optimal Interpolation (OI) technique

²The unusually long delay is due to the automatic scanner calibration routine run at the beginning of each scan cycle.

³This system did not have ability to trigger scans at prescribed times.

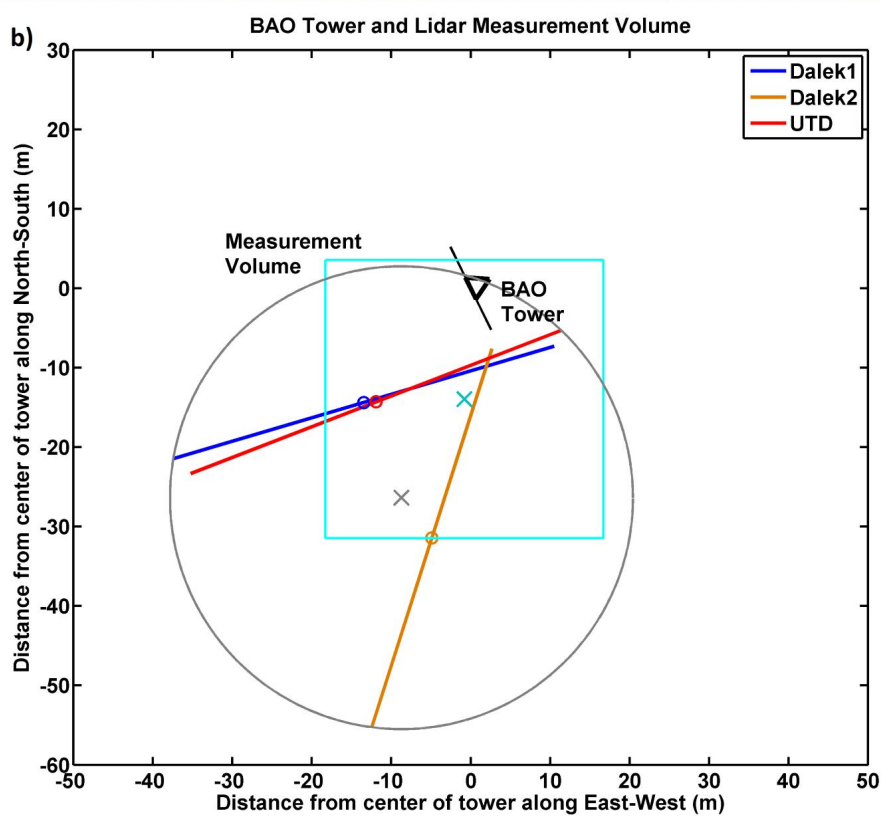
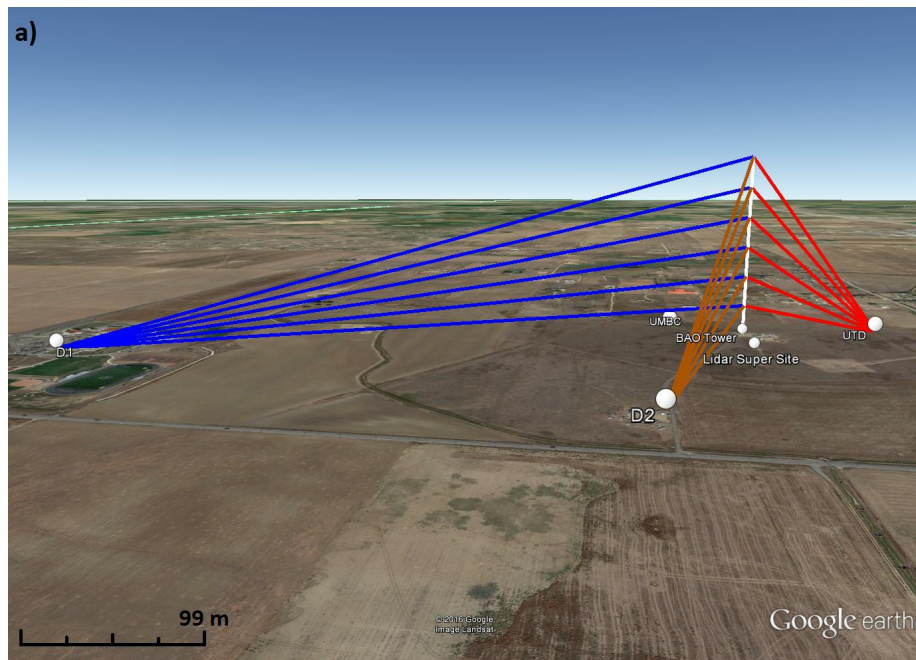


188 *2.1 Virtual Tower Stares:*

189 The virtual tower stare (VTS) scan pattern involves interrogating a common volume
190 using multiple Doppler lidars at pre-defined heights at a given location to form a “virtual tower”
191 (Calhoun et al., 2006; Fuertes et al., 2014; Gunter et al., 2015; Newman et al., 2016). A
192 schematic of the triple lidar VTS scan tested during the XPIA field experiment is shown in
193 Figure 2a. Each of the three 200S lidars (D1, D2 and UTD) performed a temporally correlated
194 25-s stare at each of the 6 sonic anemometer level (50 m to 300 m with 50 m increments) and
195 therefore creating a virtual tower of wind measurements every 3-mins. The LOS velocities that
196 fall within the common volume are least-squares fitted using Eq. 1 (Fuertes et al., 2014) to
197 estimate the three-dimensional wind velocity.

198 The common volume is defined as a square (cyan box in Figure 2b) 35 m on a side and
199 10 m in the vertical centered at each of the sonic height levels with its center 10 m south of the
200 southeast sonic anemometer on the BAO tower (this was the closest position to the tower that
201 allowed overlapping measurements without blockage). As observed from Figure 2b, the
202 effective measurement volume (defined as the circle enveloping the outer-most range-gate
203 points) is slightly larger with a diameter of 60 m. It is also seen from Figure 2b that the look
204 directions of D1 and UTD are close to 180 degrees apart. This non-ideal setup for triple Doppler
205 measurements was dictated by logistics of deployment. However, the UTD lidar makes
206 measurements with much steeper elevation angles compared to D1 and hence does provide
207 additional information for wind retrieval.

208





210 Figure 2. The Virtual Tower Stares Scan. (a) Schematic of the VTS technique. The blue, red and
211 orange lines indicate beams from each of the three 200S lidars that make measurements at each
212 sonic anemometer level. (b) Location and size of the common volume (cyan box) with respect to
213 the BAO tower. The blue, red and orange lines are range-gates from the three 200S lidars that
214 fall within the common volume. The grey circle indicates the estimated measurement volume
215 defined by the position of the range-gates.

216

217 Similar virtual towers were performed at two other locations to compare with other
218 instrumentation deployed during XPIA. Therefore the repeat period for these virtual towers
219 discussed here is once every 10-mins. The 25-s stare period was chosen to ensure that all three
220 200S lidars were measuring the common volume simultaneously. However, the 3-D wind
221 retrieval was made using 5-s of spatially and temporally overlapping LOS velocity data.

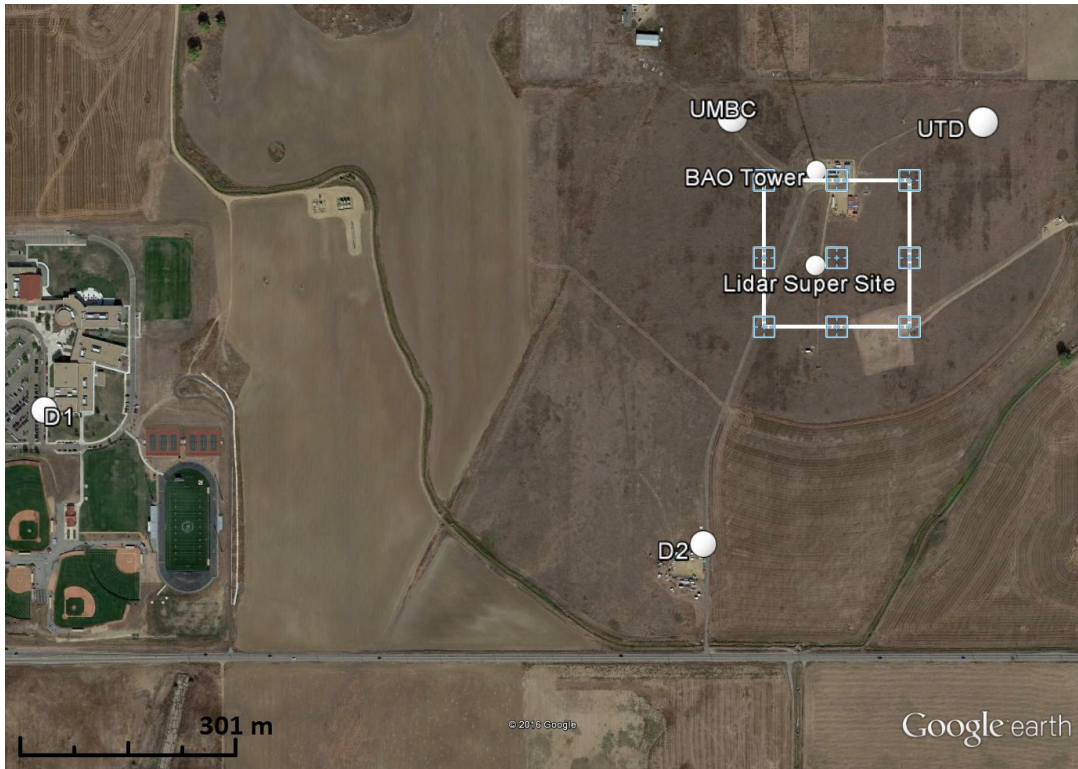
222

223 2.2 Coordinated Sparse Sampling:

224 While VTS scan provides a profile of wind velocity at any given location, wind velocity
225 measurements can also be performed over horizontal planes through temporally and spatially
226 coordinated scans that interrogate common volumes on a horizontal plane. One limitation to
227 making measurements over a large enough area using contiguous volumes is the time required to
228 simultaneously interrogate this area using coordinated scanning. The time required to complete a
229 scan is determined by the data rate of the lidar systems, overlap period and the geometry defined
230 by the instrument locations. Given the instrument locations during XPIA and data rate
231 limitations of the 200S lidars, the time required to sample an area through contiguous
232 measurement points would be too large to sample a feature sufficiently before it advected out of
233 the measurement domain. Therefore, to reduce the time required to make such a measurement,
234 sparse sampling strategies were considered. The sparse sampling technique discussed in this
235 paper is called Small Checkerboard (SCB) scan and the layout of this technique is shown in
236 Figure 3. The scanning strategy involved sampling a 3x3 grid covering a horizontal area of
237 approximately 150 m x 150 m and 100 m above the ground. The three lidars paused 5 seconds at
238 each grid point and hence completed one SCB scan every 1 minute. This measurement strategy
239 was carried out using the D1, D2 and UTD scanning 200S lidars for a period of 9 days.



240



241

242 Figure 3. Schematic of the Small Checkerboard (SCB) scan. The white outline shows the
243 domain over which measurements are made and the blue squares indicate the locations of
244 measurement volumes interrogated by the scanning Doppler lidars.

245

246 2.3 Uncoordinated Triple-Doppler Virtual Tower

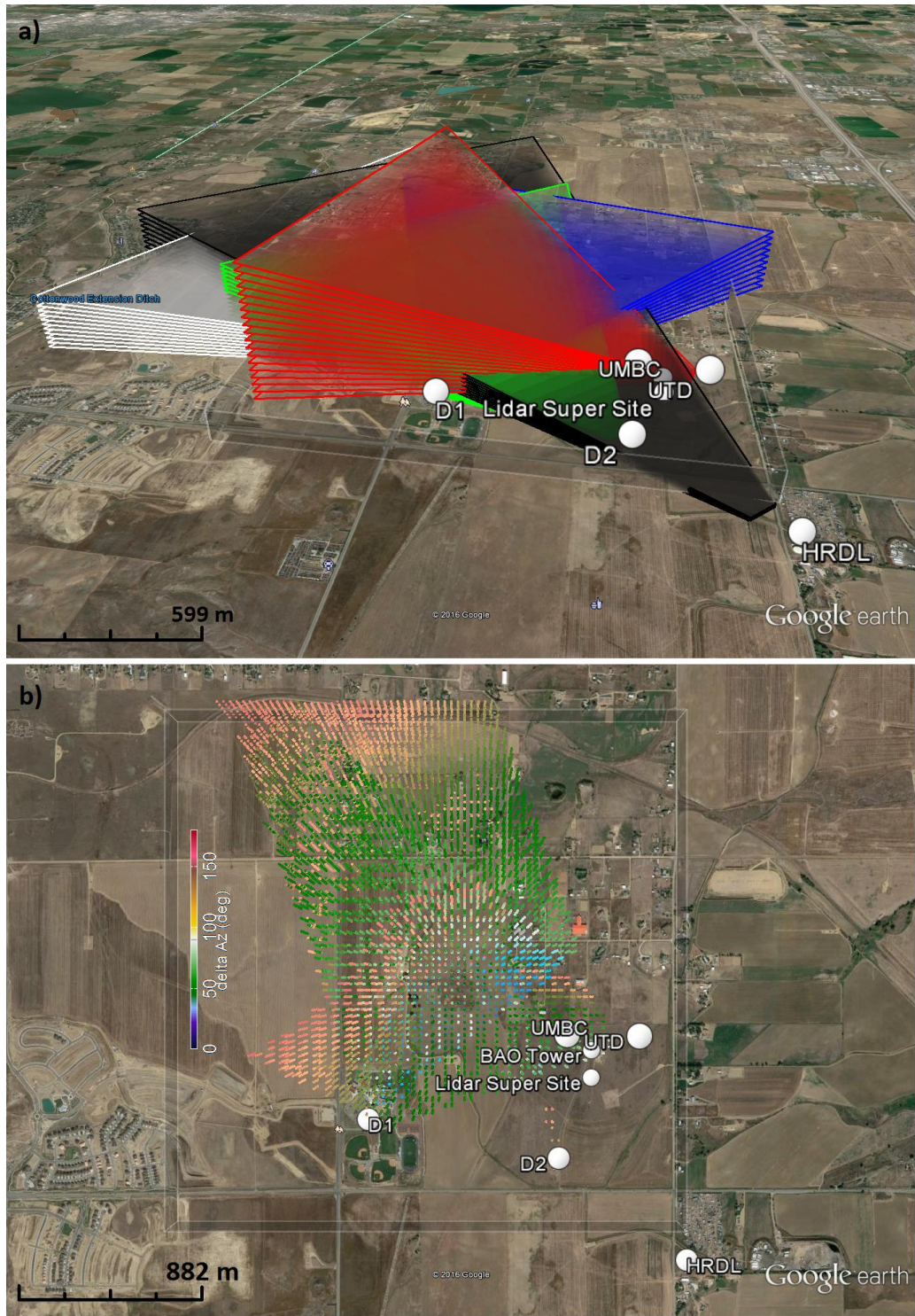
247 This measurement technique is similar to the one explained in Section 2.1 in that three
248 Doppler lidars scan a common volume to make three-dimensional wind field measurements.
249 However, in order to reduce the time required to perform a virtual tower and increase the update
250 rates, the lidars performed continuous temporally uncoordinated RHI scans at the BAO tower
251 location. Each RHI scan takes 15 seconds to perform and hence a three-dimensional wind field
252 measurement can be made every 15 seconds, compared to 3 minutes required for the VTS
253 technique. The trade-off is that not all lidars are looking at the same volume simultaneously. The
254 three dimensional wind field is estimated by least-squares fitting to Eq. 1 the LOS velocity



255 measurements from the three 200S lidars (D1, D2 and UTD) that fall within the common volume
256 (50 m on a side and 10 m in the vertical) and within a 15-s time window. The three 200S lidars
257 performed intersecting RHI scans at three locations (including near the BAO tower) for 20
258 minutes at each location before repeating the sequence again. This measurement strategy was
259 performed for a period of approximately 2 days.

260 *2.4 Uncoordinated Multi-Doppler Volume Scan:*

261 With the uncoordinated multi-Doppler measurement technique, the constraint that
262 multiple lidars need to interrogate a common volume simultaneously is removed allowing to
263 speed up sampling of the domain of interest. In this measurement technique, five Doppler lidars
264 (HRDL, D1, D2, UTD and UMBC) performed a set of complementary PPI scans that would
265 ensure that at least two Doppler beams overlapped within each grid point (defined as 50 m on a
266 side in the horizontal and 15 m in the vertical) within a 5 minute update period. This scan
267 strategy resulted in a grid which approximately 1.5 km x 1 km in the horizontal and covered
268 heights 30 m to 300 m above the ground with 15 m vertical resolution. A representation of the
269 scans performed by each of the scanning lidars and the resulting grid is shown in Figure 4.





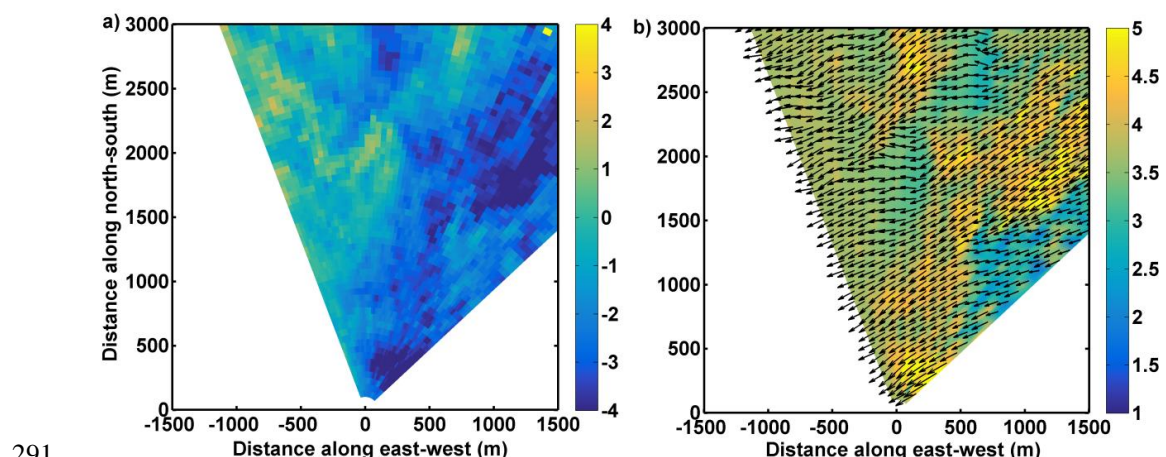
271 Figure 4. Scans performed by each of the scanning Doppler lidars to produce a 3-D volume of
272 horizontal wind field. (a) Representation of the PPI sector scans performed by each lidar. (b)
273 Grid points that have LOS velocities from at least two lidars and the colors indicate difference in
274 azimuth between their respective look directions.

275

276 Important consideration in the scan design for this experiment were the limitations on
277 lidar siting and ensuring overlap with the BAO in order to validate the wind measurements. This
278 constraint resulted in the measurement volume being quite close to the Doppler lidars and hence
279 required steep elevation angles and several PPI sectors to cover the volume of interest. These
280 consideration resulted with the spatial coverage and the update rates reported in this paper.
281 Ideally, this type of measurement would be performed with the Doppler lidars further away from
282 the domain of interest so that shallower elevation PPI scans can be employed which can help
283 cover larger areas with faster update rates.

284 *2.5 Single Doppler Velocity Retrievals:*

285 The single Doppler retrieval technique investigated in this paper is the Optimal
286 Interpolation (OI) technique (Choukulkar et al., 2012). The OI technique allows retrieval of 2-D
287 wind fields over PPI scans without assumption of spatial homogeneity of the wind field. The
288 spatial variability information in the LOS velocity field is thus preserved which can be useful to
289 study complex flows such as flow in and near wind farms and in complex terrain. An example
290 retrieval of the horizontal wind field using this technique is shown in Figure 5.





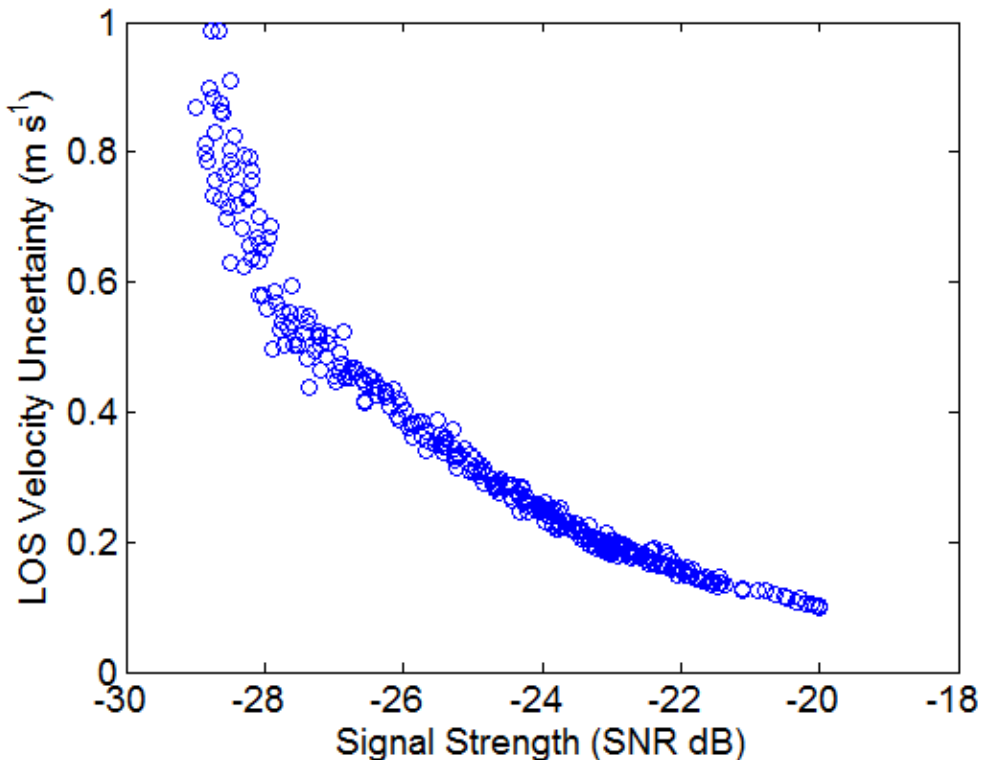
292 Figure 5. OI retrieval of the horizontal wind field on a PPI scan performed by D1 on April 25th,
293 1652 UTC. (a) LOS velocity field (in m s^{-1}) measured by D1 (b) Horizontal wind field retrieved
294 using the OI technique. The colors indicate magnitude of horizontal wind speed (in m s^{-1}) and
295 wind direction is indicated by arrows.

296

297 The OI technique uses Bayesian statistical technique to find a 2-D wind field most
298 consistent with the LOS velocity observations from the lidar PPI scans. The technique starts
299 with a first guess (referred to as “background”) of the wind field which is a single VAD estimate
300 using all the LOS velocities from the PPI scan. The final wind field is arrived at by adding an
301 “analysis increment” to the first guess which is estimated using the background and observation
302 error covariances (see Choukulkar et al. (2012b) for details). The OI technique does not make
303 any assumptions about the flow field (such as homogeneity or isotropy), however, it assumes that
304 the background error is homogeneous. The validity of this assumption has been tested through
305 simulated lidar measurements and was found to be reasonable (Choukulkar, 2013).

306 **3. Determining Baseline Uncertainty:**

307 Uncertainties emerge associated with the LOS velocity measurements made by the
308 Doppler lidar. These uncertainties can be categorized into: (1) random error in the estimation of
309 the velocity and (2) error due to the path integration (range-gating) inherent in pulsed Doppler
310 lidar measurements. The random component of the LOS velocity estimate, for D1, found by
311 linearly fitting the autocovariance from lags 1 through 4 and extrapolating to zeroth lag
312 (Lenschow et al., 2000) is shown in Figure 6. Similar values were estimated for all three 200S
313 lidars (D1, D2 and UTD) and the error was a function of Signal to Noise Ratio (SNR) only.



314

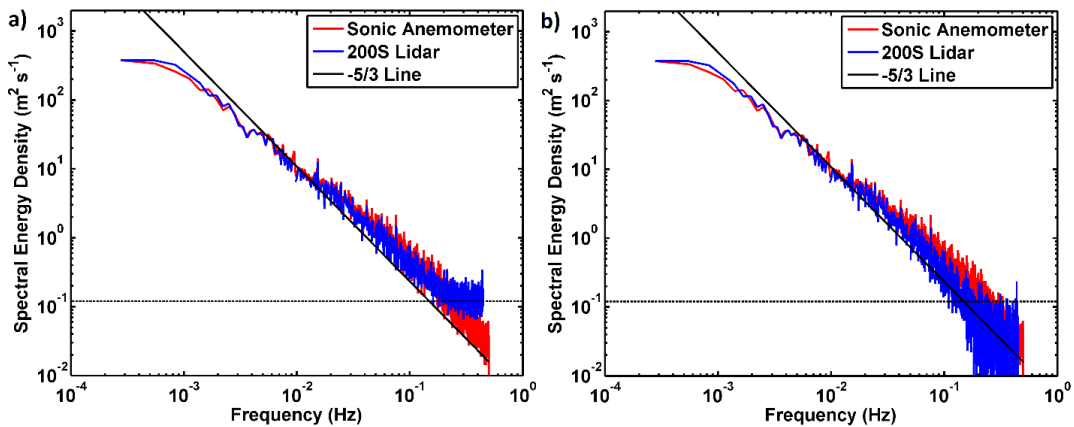
315 Figure 6. Estimate of the standard deviation of random error as a function of SNR estimated
316 using (Lenschow et al., 2000).

317

318 In addition to the uncertainty due to the random noise in the LOS velocity estimates, a
319 systematic underestimation of the variability in the velocity field at shorter length scales is
320 introduced due to the path averaging of the lidar pulse. To determine the additional uncertainty
321 due to range-gate averaging, the power spectrum of the lidar LOS velocity measurements was
322 compared to the power spectrum of the sonic-derived LOS measurements. Data from a 3-day
323 period where the 200S lidars (D1, D2 and UTD) were performing hour long stares at each sonic
324 anemometer level were used. The spectra of the lidar LOS velocity measurements from the
325 various hour long stares at each sonic anemometer level were averaged and compared to
326 correspondingly averaged sonic-derived LOS measurements (see Figure 7a). As seen in Figure
327 7a, the spectra from the lidar LOS measurements (blue line) flattens out for frequencies higher
328 than ~0.25 Hz indicating the variations due to random noise dominate. Once the variations due to



329 random noise are subtracted from the spectra, the under-prediction of the variability due to the
330 pulse averaging is clearly visible and can be estimated (see Figure 7b). This under-estimation of
331 the variability is defined as the square-root of the difference between the spectra of the sonic
332 anemometer and the lidar measurement and is found to be 0.23 m s^{-1} . The under-estimation of
333 the variability can be interpreted as a smoothing of the lidar measurements and hence adds to the
334 differences between the lidar and sonic anemometer wind measurements.



335

336 Figure 7. Comparison of the FFT of LOS data measured by the lidar and the LOS derived from
337 the sonic anemometer measurements. The solid black line indicates the energy cascade following
338 the $-5/3$ Kolmogorov energy spectrum (a) Comparison of the FFT showing the noise floor of the
339 Doppler lidar measurements (dotted black line). (b) Comparison of the FFT after subtracting the
340 noise from the lidar FFT. The under-prediction of the variability due to the pulse averaging can
341 be seen clearly and found to be 0.23 m s^{-1} .

342

343 Finally, the total difference between the 1 Hz lidar-measured-LOS velocity and the 1 Hz
344 sonic-derived-LOS velocity measurements, as estimated from direct comparison is presented in
345 Table 4 (Lundquist et al., 2016a). This difference is slightly larger than the combined
346 uncertainties from random noise and pulse averaging. This difference in the uncertainty
347 estimates could be due to some factors that are as yet unaccounted or due to improper estimate of
348 the uncertainties due to random noise and pulse averaging. The uncertainty of the LOS
349 measurement by the lidar (when compared to the sonic anemometer) allows evaluating the
350 various measurement techniques in terms of additional uncertainty added to this baseline value.



351 The offset in the LOS velocity of the UTD lidar was found to be due to improper calibration of
352 the pulse length dependent frequency offset (Lundquist et al., 2016b). This was characterized
353 using independent measurements and was found to be constant throughout the XPIA campaign.
354 Therefore in all measurements presented in this paper, this static offset has been subtracted from
355 the UTD lidar LOS velocity.

356

357 Table 4. Comparison of the instantaneous lidar LOS measurement to sonic derived LOS
358 measurement at all sonic levels.

Lidar	Corr Coef.	Slope	Offset	Std. Dev. of differences
D1	0.99	1.01	0.02 m s ⁻¹	0.50 m s ⁻¹
D2	0.98	0.98	-0.12 m s ⁻¹	0.66 m s ⁻¹
UTD	0.99	1.00	-0.60 m s ⁻¹	0.53 m s ⁻¹

359

360 4. Validation of Wind-field Measurements:

361 The wind field measurements from the measurement techniques outlined earlier are now
362 evaluated using the sonic anemometer as the standard. A three-step 6-sigma outlier rejection is
363 applied in each of the comparisons before estimating the validation metrics. The validation
364 metrics used here are the mean and standard deviation of the differences between the lidar and
365 sonic anemometer measurements.

366 4.1 Virtual Tower Stares:

367 The 3-dimensional wind was measured using the VTS technique by taking 5-s of LOS
368 velocity data from the three 200S lidars which overlapped in time and space (as defined by the
369 common volume), and least-squares fitted to Eq. 1 to derive the 3-D wind field. The comparisons
370 of the 3-dimensional wind field as measured by the VTS technique to 5-s averaged sonic
371 anemometer measurements is shown in Table 5. These measurements agree with a high
372 correlation coefficient (0.97 and 0.99 for wind speed and direction respectively) and low
373 standard deviation of the differences (0.51 m s⁻¹ and 10.16° for horizontal wind speed and
374 horizontal wind direction respectively) between the sonic anemometer and the VTS
375 measurements. In addition, the vertical velocity measurements also show a reasonably good
376 correlation coefficient (0.86) and low standard deviation of differences (0.5 m s⁻¹). Note that in



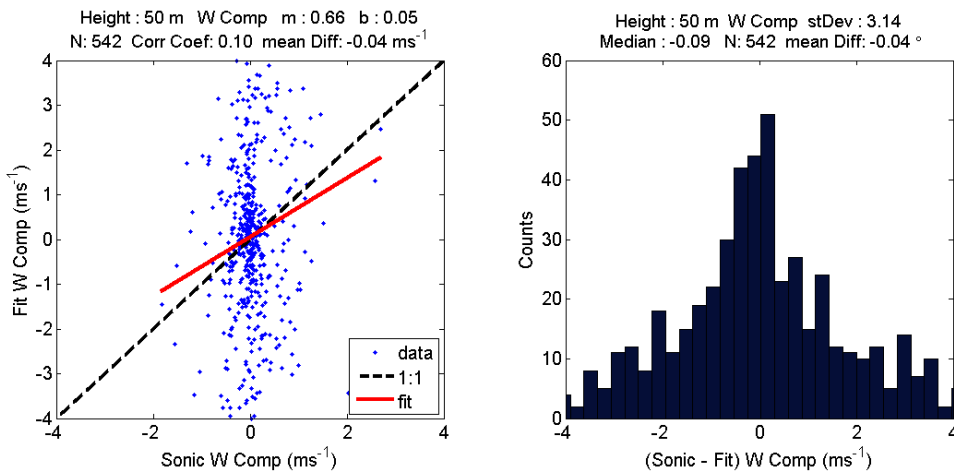
377 the vertical velocity comparisons, only measurements at and above the 150 m sonic are
 378 compared. This is due to the fact that at the lower sonic levels, the elevation angles in the VTS
 379 scans were quite low and as a result the component we are trying to estimate is perpendicular to
 380 the lidar look direction resulting in a noisy vertical velocity retrieval. The velocity retrievals at
 381 the 50 m level from the VTS scans are shown in Figure 8. As can be observed from Figure 8,
 382 there is no skill in the vertical velocity retrievals at low elevation angles.

383 Table 5. Statistics from comparison of wind field measurements from the VTS to the sonic
 384 anemometer measurements

Wind Field	Corr Coef	Slope	Offset	Std Dev of Differences
Horizontal Wind Speed (all heights)	0.97	0.96	0.21 m s ⁻¹	0.50 m s ⁻¹
Horizontal Wind Direction (all heights)	0.99	0.97	3.36°	9.87°
Vertical Velocity (150 m to 300 m)	0.86	1.06	-0.02 m s ⁻¹	0.50 m s ⁻¹

385

386



387

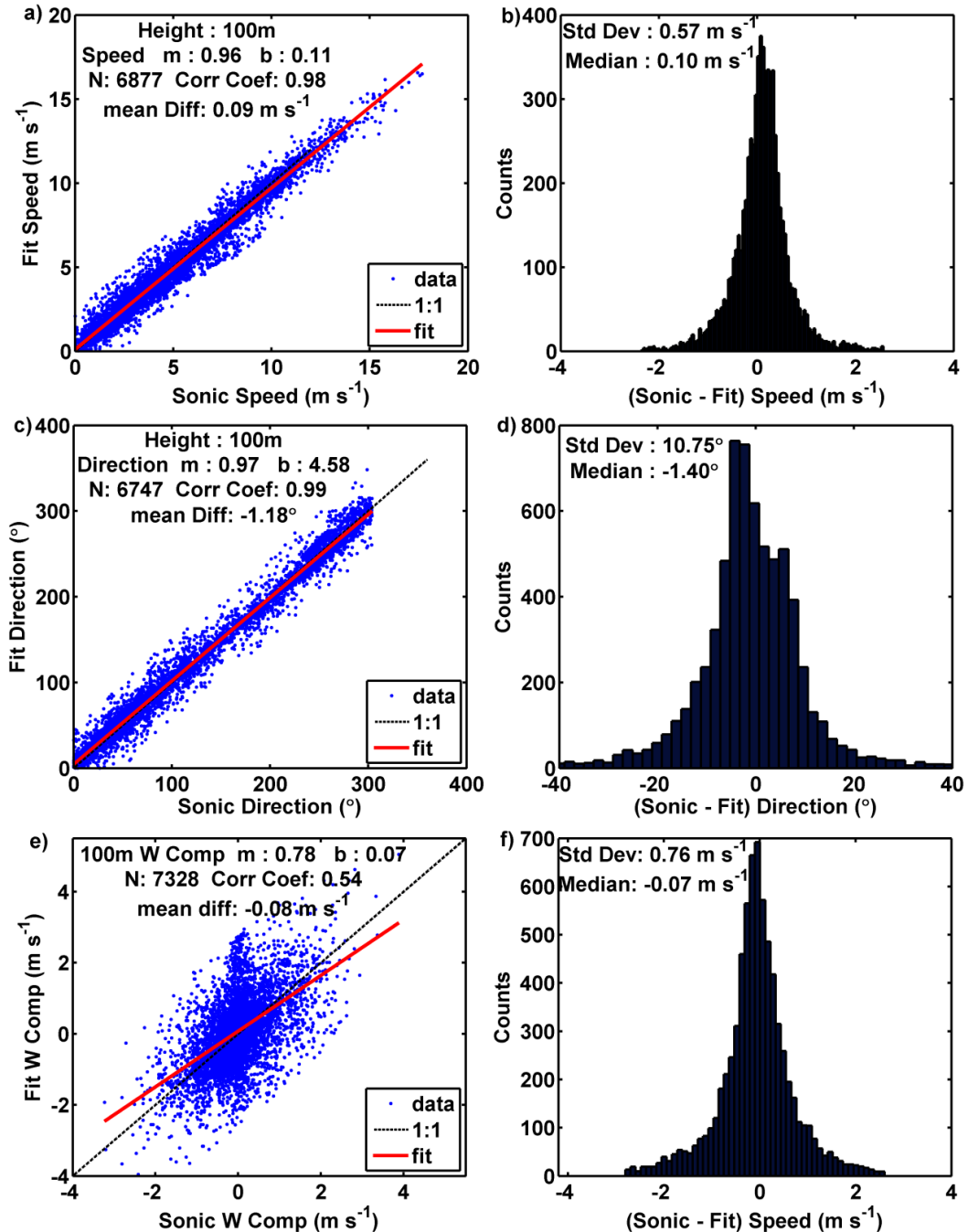
388 Figure 8. Comparison of the vertical velocity measurements from VTS at the 50 m level with
 389 the sonic anemometer measurements.

390



391 4.2 *Coordinated Sparse Sampling*:

392 The comparison of the SCB measurement point over the BAO tower with 15-s averaged
393 sonic anemometer measurements at the 100 m level are shown in Figure 9. The measurements
394 made from the SCB technique show good agreement with sonic anemometer measurements (as
395 shown in Figure 9) with correlation coefficient of 0.98 and 0.99 for wind speed and wind
396 direction respectively. The correlation coefficient for the vertical velocity was lower (0.54) due
397 to the fact that these measurements were made at the 100 m level which leads to lower skill in
398 vertical velocity measurements as explained in the previous section. The main difference
399 between the VTS measurement strategy and the SCB strategy is the amount of time buffer
400 allowed to make overlapping LOS measurements. In the VTS strategy, each lidar performed a
401 stare scan for 25-s at each measurement location, while it was 5-s for the SCB strategy.
402 Therefore, there was less time to ensure measurement overlap in the SCB strategy and it is
403 expected to have slightly higher uncertainty in wind field measurement.



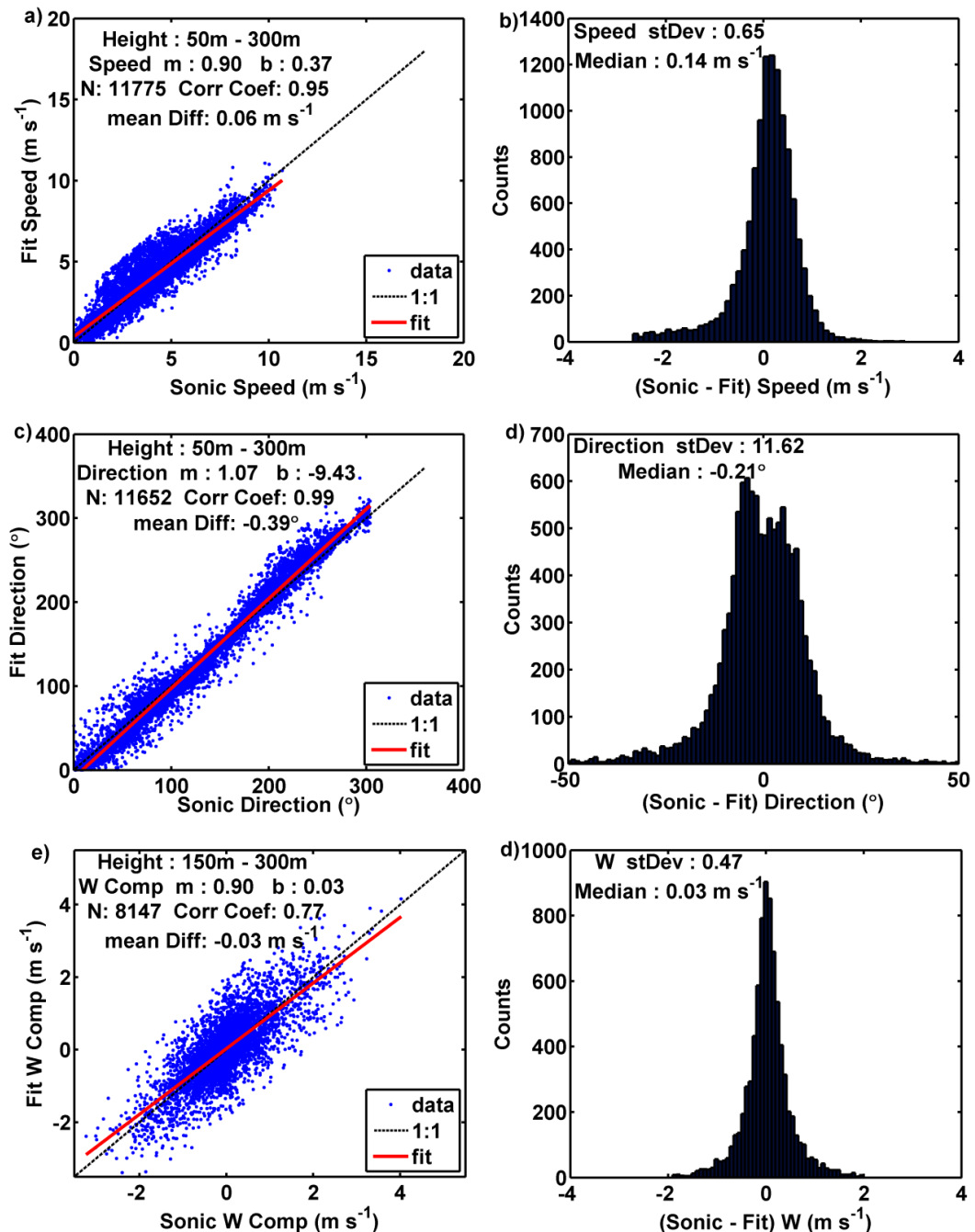
404

405 Figure 9. Comparison of the (a, b) wind speed, (c, d) wind direction and (e, f) vertical velocity
 406 measurements from the SCB technique with the measurements made by the sonic anemometer.



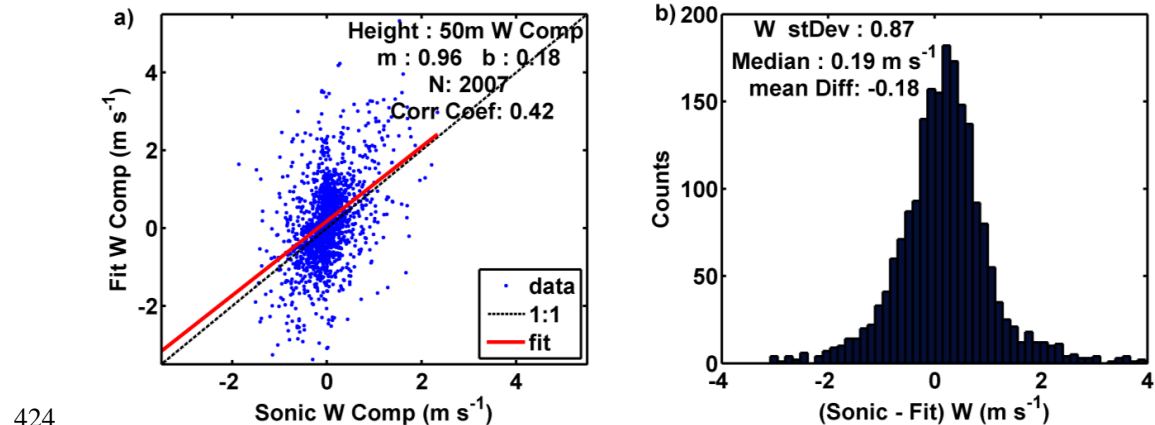
407 *4.3 Uncoordinated Virtual Towers (UVT):*

408 The measurements made from the uncoordinated virtual tower (UVT) technique were
409 compared to the 15-s averaged sonic anemometer measurements at all 6 levels of the BAO
410 tower. Figure 10 shows that the measurements from the UVT technique have good agreement
411 with the sonic anemometer measurements with correlation coefficients of 0.95 and 0.99 for wind
412 speed and wind direction respectively. The standard deviation of the differences (0.65 m s^{-1} for
413 horizontal wind speed and 11.62° for the horizontal wind direction) were found to be slightly
414 higher compared to the VTS technique. This increase is expected as the LOS velocity
415 measurements are no longer coordinated in time which leads to an increase in measurement
416 uncertainty due to non-stationarity of the atmosphere. The vertical velocity measurements made
417 using this technique for heights 150m and above show a similar skill as the VTS technique,
418 albeit with a slightly lower correlation coefficient of 0.77. In addition, comparison of the vertical
419 velocity measurements made at the 50m level (see Figure 11) show that the UVT technique has
420 no skill in making accurate measurements due to the lower elevation angles involved.



421

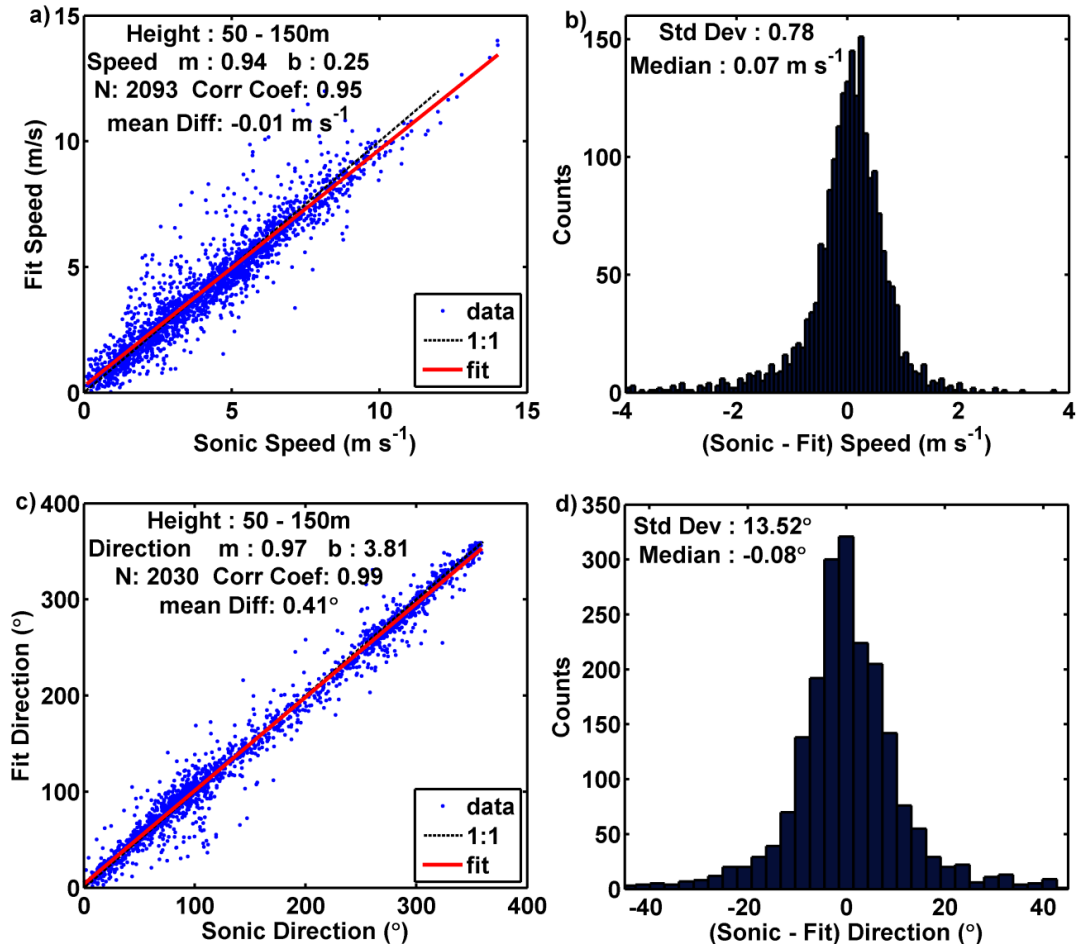
422 Figure 10. Comparison of the (a, b) wind speed, (c, d) wind direction and (e, f) vertical velocity
 423 measurements from the UVT technique with the measurements made by the sonic anemometer.



424
 425 Figure 11. Comparison of the vertical velocity measurements from UVT at the 50 m level with
 426 the sonic anemometer measurements.

427 *4.4 Uncoordinated Volume Scan:*

428 The uncoordinated volume scan strategy further relaxes the requirement for each lidar to
 429 make simultaneous LOS measurements at each measurement location and instead uses all LOS
 430 velocity measurements from all Doppler lidars that fall within the grid volume and are within a
 431 given time-window (in this case 5-min) to make a wind field measurement. Comparison of the
 432 uncoordinated volume scan measurements with 5-min averaged sonic anemometer
 433 measurements (at three levels from 50 m to 150 m), show good correlation coefficients of 0.95
 434 and 0.99 for wind speed and direction respectively (see Figure 12).



435

436 Figure 12. Comparison of the (a, b) wind speed, (c, d) wind direction measurements from the
 437 uncoordinated volume scan technique with the measurements made by the sonic anemometer.

438

439 The standard deviation of the differences between the uncoordinated volume scan
 440 measurements and sonic anemometer measurements (0.78 m s^{-1} for horizontal wind speed and
 441 13.52° for horizontal wind direction) are higher compared to the differences reported for the
 442 coordinated measurement techniques. The higher uncertainties could be due to non-stationarity
 443 of the winds over the measurement accumulation period whose effect is expected to be much
 444 larger compared to the case of UVT technique due to the longer measurement accumulation
 445 period. Another factor (which is related to the non-stationarity of the wind) is the less

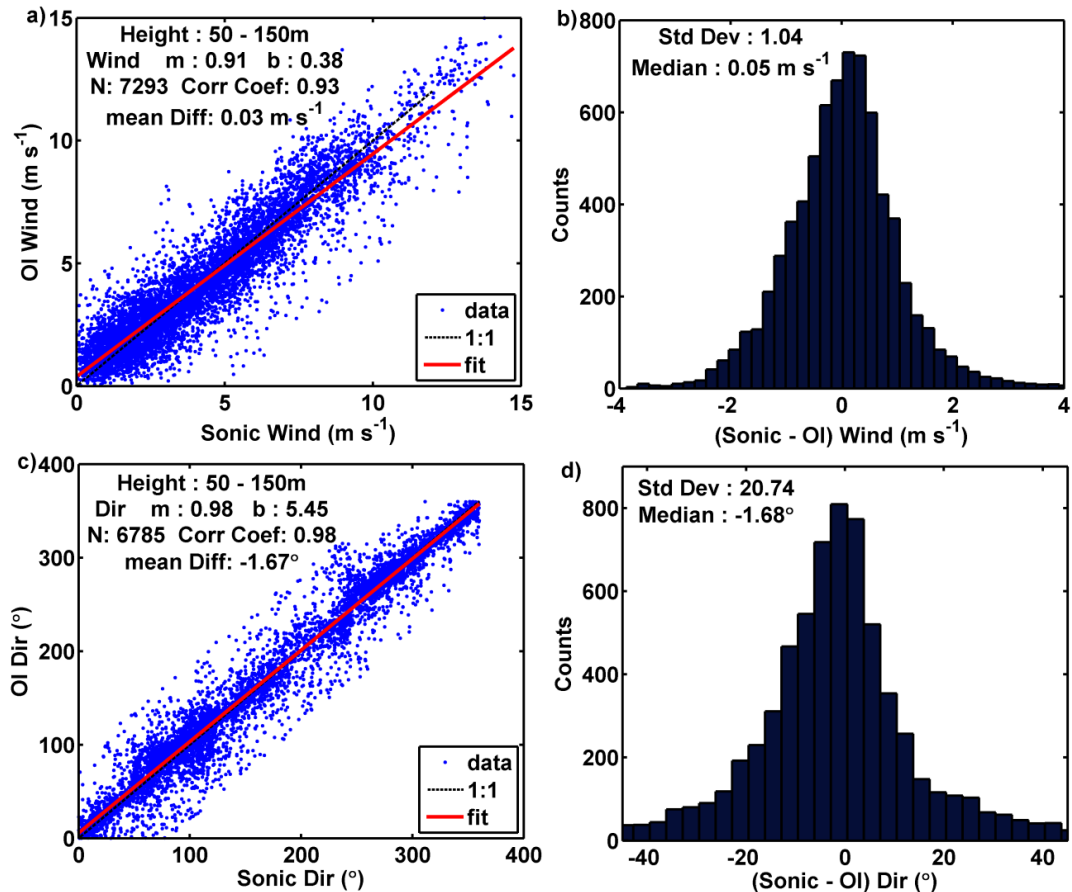


446 representative LOS velocity statistics which is due to the fact that since each lidar does not spend
447 enough time measuring within each grid cell. As a result, the mean of the LOS velocity
448 measurements from each lidar are not representative of the mean velocity over which the wind
449 retrieval is made.

450 *4.5 Single Doppler Optimal Interpolation (OI) Technique:*

451 The OI technique allows retrieval of 2-D wind field over conical scans without applying
452 the assumption of horizontal homogeneity of the wind. The OI technique was applied to the
453 sector scans performed by each lidar in the uncoordinated volume scan technique. Each sector
454 scan took 30-s to complete, and hence the OI retrieval is compared to 30-s averaged sonic
455 anemometer measurement shown in Figure 13. The retrievals from the OI technique agree with
456 the sonic anemometer measurements quite well with correlation coefficients of 0.93 and 0.98 for
457 wind speed and wind direction respectively. The standard deviation of the differences (1.04 m s^{-1}
458 ¹ for horizontal wind speed and 20.74° for horizontal wind direction) are higher, compared to the
459 uncoordinated volume scan technique.

460



461

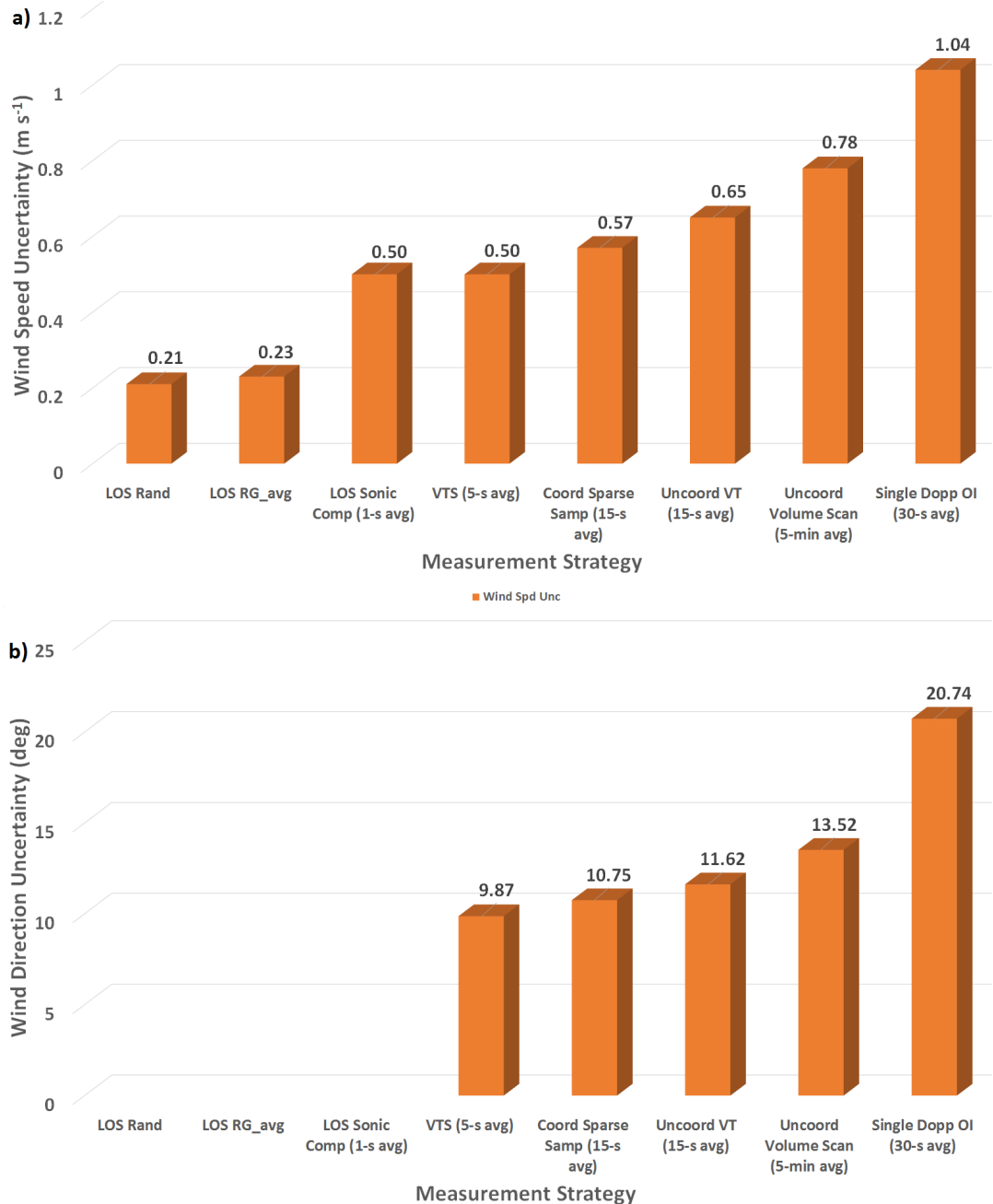
462 Figure 13. Comparison of the (a, b) wind speed, (c, d) wind direction measurements from the
 463 single Doppler OI technique with the measurements made by the sonic anemometer.

464 **5. Discussion of Results**

465 The precision of the wind measurement (defined as the standard deviation of the
 466 differences between the Doppler measurement and the sonic anemometer measurement) obtained
 467 from the various Doppler lidar techniques can now be compared. The measurement precision
 468 reported for each of the techniques is related to time it takes to perform one measurement, and
 469 hence the time average used to evaluate the technique. This method is chosen so that the
 470 inherent trade-off between spatial coverage and temporal resolution is clear.



471 Figure 14 shows the comparison of the uncertainties for the LOS velocity as well as the
472 estimates of the horizontal wind speed and direction from the various measurement techniques.
473 As seen from Figure 14, the uncertainty in the LOS velocity (from comparison with sonic
474 anemometer) is 0.5 m s^{-1} . It is observed that with an averaging time of 5-s for the VTS method,
475 the uncertainty does not increase compared to the sonic-LOS velocity uncertainty. The most
476 probable reason the precision of the VTS technique is found to be the highest (compared to other
477 velocity retrieval techniques presented here) is due to the fact that the three 200S lidars made
478 simultaneous measurements within the common volume and thus relying less heavily on the
479 assumption of stationarity of the atmosphere or spatial homogeneity. Increasing the
480 measurement complexity and spatial coverage either through faster scanning or relaxing the
481 requirement of temporal coordination, the measurement uncertainty increases as well. While the
482 single Doppler OI does not require complex scanning technique, it requires certain assumptions
483 as part of the retrieval process (Choukulkar et al., 2012) and hence increases the measurement
484 uncertainty.



485

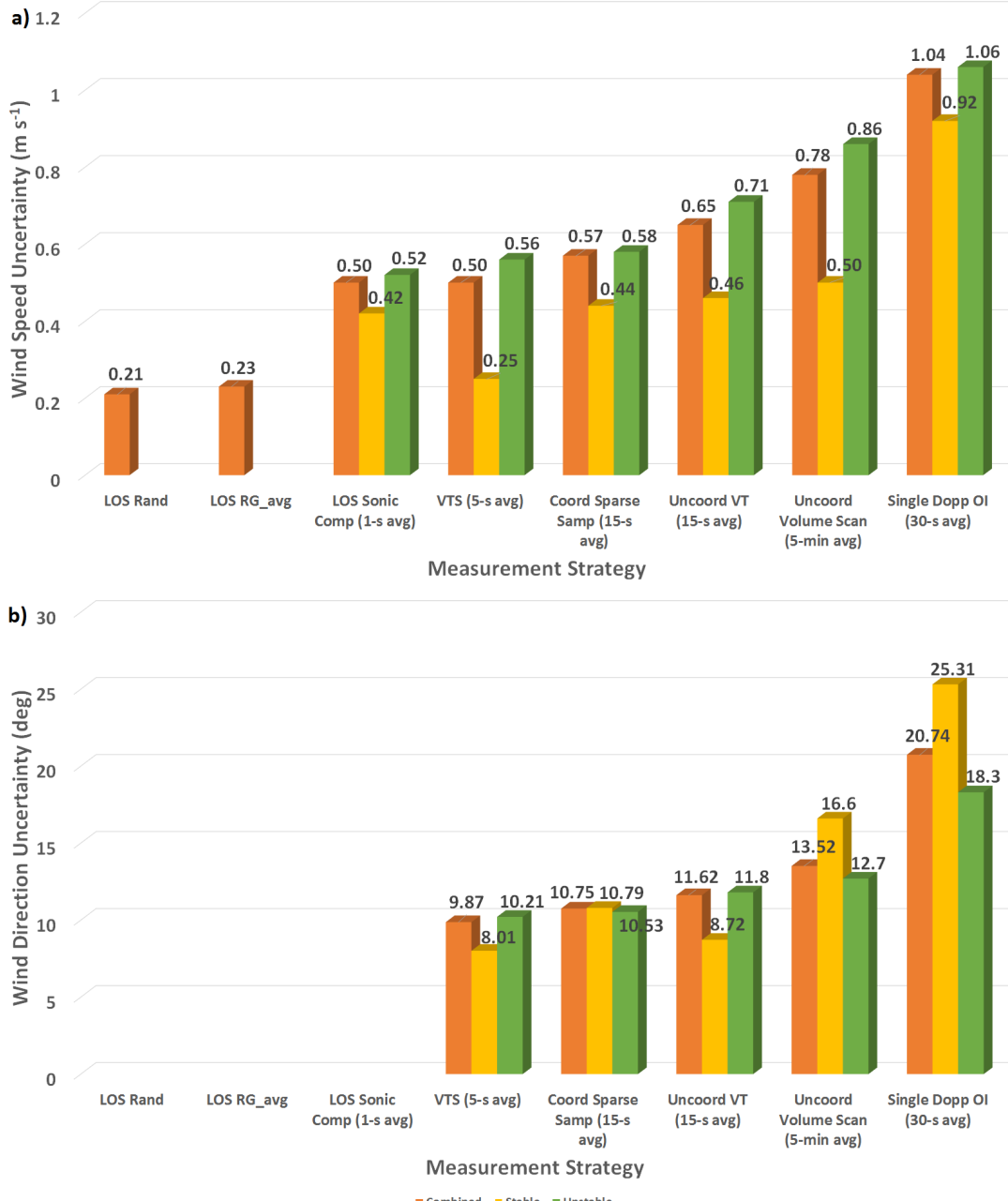
486 Figure 14. Measurement uncertainties for (a) horizontal wind speed and (b) horizontal wind
 487 direction estimated for the different measurement strategies investigated.



488 *Effect of Stability:*

489 The precision of wind measurements is also evaluated in various stability conditions.
490 The stability is defined using hourly averaged virtual potential temperature gradient between the
491 50 m level and the 300 m level using both the tower measurements and radiometer
492 measurements (Bianco et al., 2016). Conditions were determined to be stable for positive
493 gradient of the virtual potential temperature and unstable for a negative gradient of the virtual
494 potential temperature.

495 The lidar wind speed measurements are found to be slightly more precise during stable
496 conditions, compared to unstable conditions (see Figure 15). The higher uncertainties observed
497 during unstable conditions might be due to the fact that unstable conditions show higher
498 variability than stable conditions which might lead to higher level of uncertainty. However, no
499 consistent pattern emerges for the effect of stability on wind direction uncertainty. This might be
500 due to the fact that all the stable conditions examined here were accompanied by low wind
501 conditions which usually leads to higher variability in wind direction while the unstable
502 conditions had higher wind speeds. As a result, the wind direction uncertainty during stable
503 conditions is found to be higher. It is clear from Figure 15 that stability and spatial variability do
504 have a significant impact on the measurement uncertainty.



505

506 Figure 15. Measurement uncertainty as a function of stability for (a) horizontal wind speed and
 507 (b) horizontal wind direction.

508



509 **6. Conclusions**

510 Scanning Doppler lidars are powerful tools that enable measuring atmospheric flows
511 using various configuration of single and multi-Doppler techniques. An important aspect of
512 proper interpretation of the measurements made using Doppler lidars is understanding the
513 inherent uncertainties associated with the corresponding measurement technique. In this paper,
514 the uncertainties associated with Doppler lidar measurements were quantified starting with the
515 uncertainties due to random noise and pulse averaging to uncertainties associated with single and
516 multi-Doppler measurement techniques.

517 It was found that as complexity of the measurement technique and/or the spatial coverage
518 of measurements made increased, the uncertainty in the wind measurement also increased. For
519 multi-Doppler measurements, the magnitude of uncertainty was associated with ability to make
520 coordinated measurements. Measurements made using accurate coordinated scanning resulted in
521 lower uncertainties compared to measurements from temporally uncoordinated scanning. This
522 result is expected due to the non-stationarity of the atmosphere and presence of spatial variability
523 in the wind field. The single Doppler OI technique resulted in the highest measurement
524 uncertainty (compared to multi-Doppler techniques), but also had the largest spatial coverage at
525 high update rates and is less expensive as a result of requiring only one lidar.

526 The results illustrate the trade-off between making highly precise measurements at one
527 location versus accepting a lower precision but covering larger spatial extents. Although the
528 magnitude of the uncertainties for the various measurement techniques presented in this paper
529 might not be reproducible at other locations and under different wind conditions, the trends
530 observed should be similar. This quantification of the uncertainty as a function of measurement
531 technique allows proper selection of measurement strategy given the goals of the experiment and
532 interpretation of the measurements made using those techniques.

533 **7. Acknowledgements**

534 The authors acknowledge the funding for this work provided by the U.S. Department of
535 Energy, Office of Energy Efficiency and Renewable Energy and by NOAA's Earth System
536 Research Laboratory. The authors also acknowledge contributions of numerous individuals and
537 organization who assisted with the field deployment including Bruce Bartram, Duane Hazen,
538 Tom Ayers, Jesse Leach, Paul Johnston, Lefthand Water District, Erie High School and the St.



539 Vrain School District. We also express our appreciation to NOAA/Earth Systems Research
540 Laboratory/Physical Sciences Division for supporting the instrumentation at the BAO facility.
541 We express appreciation to the National Science Foundation for supporting the CABL
542 deployments (https://www.eol.ucar.edu/field_projects/cabl) of the tower instrumentation. NREL
543 is a national laboratory of the U. S. Department of Energy, Office of Energy Efficiency and
544 Renewable Energy, operated by the Alliance for Sustainable Energy, LLC.

545

546 8. References:

547 Banta, R. M., Pichugina, Y. L., Brewer, W. A., Lundquist, J. K., Kelley, N. D., Sandberg, S. P.,
548 Alvarez II, R. J., Hardesty, R. M. and Weickmann, A. M.: 3D Volumetric Analysis of Wind
549 Turbine Wake Properties in the Atmosphere Using High-Resolution Doppler Lidar, *J. Atmospheric Ocean. Technol.*, 32(5), 904–914, doi:10.1175/JTECH-D-14-00078.1, 2015.

550 Barlow, J. F., Dunbar, T. M., Nemitz, E. G., Wood, C. R., Gallagher, M. W., Davies, F.,
551 O'Connor, E. and Harrison, R. M.: Boundary layer dynamics over London, UK, as observed
552 using Doppler lidar during REPARTEE-II, *Atmospheric Chem. Phys.*, 11(5), 2111–2125, 2011.

553 Berg, J., Vasiljević, N., Kelly, M., Lea, G. and Courtney, M.: Addressing Spatial Variability of
554 Surface-Layer Wind with Long-Range WindScanners, *J. Atmospheric Ocean. Technol.*, 32(3),
555 518–527, doi:10.1175/JTECH-D-14-00123.1, 2015.

556 Bianco, L., Friedrich, K., Wilczak, J. M., Hazen, D., Wolfe, D., Delgado, R., Oncley, S. P. and
557 Lundquist, J. K.: Assessing the accuracy of microwave radiometers and radio acoustic sounding
558 systems for wind energy applications, *Atmospheric Meas. Tech.*, 2016.

560 Bingöl, F., Mann, J. and Foussekis, D.: Conically scanning lidar error in complex terrain,
561 *Meteorol. Z.*, 18(2), 189–195, doi:10.1127/0941-2948/2009/0368, 2009.

562 Browning, K. A. and Wexler, R.: The determination of kinematic properties of a wind field using
563 Doppler radar, *J. Appl. Meteorol.*, 7(1), 105–113, 1968.

564 Calhoun, R., Heap, R., Princevac, M., Newsom, R., Fernando, H. and Ligon, D.: Virtual towers
565 using coherent Doppler lidar during the Joint Urban 2003 dispersion experiment, *J. Appl.*
566 *Meteorol. Climatol.*, 45(8), 1116–1126, 2006.

567 Chan, P. W. and Shao, A. M.: Depiction of complex airflow near Hong Kong International
568 Airport using a Doppler LIDAR with a two-dimensional wind retrieval technique, *Meteorol. Z.*,
569 16(5), 491–504, 2007.

570 Cherukuru, N. W., Calhoun, R., Lehner, M., Hoch, S. W. and Whiteman, C. D.: Instrument
571 configuration for dual-Doppler lidar coplanar scans: METCRAX II, *J. Appl. Remote Sens.*, 9(1),
572 96090–96090, 2015.



573 Choukulkar, A.: Coherent Doppler Lidar for Boundary Layer Studies and Wind Energy, in ASU
574 Electronic Dissertations and Theses, Arizona State University. [online] Available from:
575 <http://hdl.handle.net/2286/R.I.16449>, 2013.

576 Choukulkar, A., Calhoun, R., Billings, B. and Doyle, J. D.: A modified optimal interpolation
577 technique for vector retrieval for coherent Doppler lidar, *Geosci. Remote Sens. Lett. IEEE*, 9(6),
578 1132–1136, 2012.

579 Collier, C. G., Davies, F., Bozier, K. E., Holt, A. R., Middleton, D. R., Pearson, G. N., Siemen,
580 S., Willetts, D. V., Upton, G. J. G. and Young, R. I.: Dual-Doppler Lidar Measurements for
581 Improving Dispersion Models, *Bull. Am. Meteorol. Soc.*, 86(6), 825–838, doi:10.1175/BAMS-
582 86-6-825, 2005.

583 Damian, T., Wieser, A., Träumner, K., Corsmeier, U. and Kottmeier, C.: Nocturnal Low-level
584 Jet Evolution in a Broad Valley Observed by Dual Doppler Lidar, *Meteorol. Z.*, 305–313, 2014.

585 Drechsel, S., Mayr, G. J., Chong, M., Weissmann, M., Dörnbrack, A. and Calhoun, R.: Three-
586 Dimensional Wind Retrieval: Application of MUSCAT to Dual-Doppler Lidar, *J. Atmospheric
587 Ocean. Technol.*, 26(3), 635–646, doi:10.1175/2008JTECHA1115.1, 2009.

588 Fernando, H. J. S., Pardyjak, E. R., Di Sabatino, S., Chow, F. K., De Wekker, S. F. J., Hoch, S.
589 W., Hacker, J., Pace, J. C., Pratt, T., Pu, Z., Steenburgh, W. J., Whiteman, C. D., Wang, Y.,
590 Zajic, D., Balsley, B., Dimitrova, R., Emmitt, G. D., Higgins, C. W., Hunt, J. C. R., Knievel, J.
591 C., Lawrence, D., Liu, Y., Nadeau, D. F., Kit, E., Blomquist, B. W., Conry, P., Coppersmith, R.
592 S., Creegan, E., Felton, M., Grachev, A., Gunawardena, N., Hang, C., Hocut, C. M., Huynh, G.,
593 Jeglum, M. E., Jensen, D., Kulandaivelu, V., Lehner, M., Leo, L. S., Liberzon, D., Massey, J. D.,
594 McEnerney, K., Pal, S., Price, T., Sghiatti, M., Silver, Z., Thompson, M., Zhang, H. and
595 Zsedorovits, T.: The MATERHORN: Unraveling the Intricacies of Mountain Weather, *Bull. Am.
596 Meteorol. Soc.*, 96(11), 1945–1967, doi:10.1175/BAMS-D-13-00131.1, 2015.

597 Fuertes, F. C., Iungo, G. V. and Porté-Agel, F.: 3D Turbulence Measurements Using Three
598 Synchronous Wind Lidars: Validation against Sonic Anemometry, *J. Atmospheric Ocean.
599 Technol.*, 31(7), 1549–1556, doi:10.1175/JTECH-D-13-00206.1, 2014.

600 Gunter, W. S., Schroeder, J. L. and Hirth, B. D.: Validation of Dual-Doppler Wind Profiles with
601 in situ Anemometry, *J. Atmospheric Ocean. Technol.*, 32(5), 943–960, doi:10.1175/JTECH-D-
602 14-00181.1, 2015.

603 Hill, M., Calhoun, R., Fernando, H. J. S., Wieser, A., Dörnbrack, A., Weissmann, M., Mayr, G.
604 and Newsom, R.: Coplanar Doppler lidar retrieval of rotors from T-REX, *J. Atmospheric Sci.*,
605 67(3), 713–729, 2010.

606 Kaimal, J. C. and Gaynor, J. E.: The Boulder Atmospheric Observatory, *J. Clim. Appl.
607 Meteorol.*, 22(5), 863–880, doi:10.1175/1520-0450(1983)022<0863:TBAO>2.0.CO;2, 1983.

608 Käsler, Y., Rahm, S., Simmet, R. and Kühn, M.: Wake Measurements of a Multi-MW Wind
609 Turbine with Coherent Long-Range Pulsed Doppler Wind Lidar, *J. Atmospheric Ocean.
610 Technol.*, 27(9), 1529–1532, doi:10.1175/2010JTECHA1483.1, 2010.



611 Klein, P., Bonin, T. A., Newman, J. F., Turner, D. D., Chilson, P. B., Wainwright, C. E.,
612 Blumberg, W. G., Mishra, S., Carney, M., Jacobsen, E. P., Wharton, S. and Newsom, R. K.:
613 LABLE: A Multi-Institutional, Student-Led, Atmospheric Boundary Layer Experiment, Bull.
614 Am. Meteorol. Soc., 96(10), 1743–1764, doi:10.1175/BAMS-D-13-00267.1, 2015.

615 Krishnamurthy, R., Choukulkar, A., Calhoun, R., Fine, J., Oliver, A. and Barr, K. S.: Coherent
616 Doppler lidar for wind farm characterization, Wind Energy, 16(2), 189–206, 2013.

617 Lenschow, D. H., Wulfmeyer, V. and Senff, C.: Measuring second-through fourth-order
618 moments in noisy data, J. Atmospheric Ocean. Technol., 17(10), 1330–1347, 2000.

619 Lundquist, J. K., Churchfield, M. J., Lee, S. and Clifton, A.: Quantifying error of lidar and sodar
620 Doppler beam swinging measurements of wind turbine wakes using computational fluid
621 dynamics, Atmospheric Meas. Tech., 8(2), 907–920, 2015.

622 Lundquist, J. K., Wilczak, J. M., Ashton, R., Bianco, L., Brewer, W. A., Choukulkar, A., Clifton,
623 A., Debnath, M., Delgado, R., Friedrich, K., Gunter, S., Hamidi, A., Iungo, G. V., Kaushik, A.,
624 Kosović, B., Langan, P., Lass, A., Lavin, E., Lee, J. C.-Y., McCaffrey, K. L., Newsom, R. K.,
625 Noone, D. C., Oncley, S. P., Quelet, P. T., Sandberg, S. P., Schroeder, J. L., Shaw, W. J.,
626 Sparling, L., St. Martin, C., St. Pe, A., Strobach, E., Tay, K., Vanderwende, B. J., Weickmann,
627 A., Wolfe, D. and Worsnop, R.: Assessing state-of-the-art capabilities for probing the
628 atmospheric boundary layer: the XPIA field campaign, National Renewable Energy Laboratory
629 (NREL), Golden, CO., 2016a.

630 Lundquist, J. K., Wilczak, J. M., Ashton, R., Bianco, L., Brewer, W. A., Choukulkar, A., Clifton,
631 A., Debnath, M., Delgado, R., Friedrich, K., Gunter, S., Hamidi, A., Iungo, G. V., Kaushik, A.,
632 Kosović, B., Langan, P., Lass, A., Lavin, E., Lee, J. C.-Y., McCaffrey, K. L., Newsom, R. K.,
633 Noone, D. C., Oncley, S. P., Quelet, P. T., Sandberg, S. P., Schroeder, J. L., Shaw, W. J.,
634 Sparling, L., St. Martin, C., St. Pe, A., Strobach, E., Tay, K., Vanderwende, B. J., Weickmann,
635 A., Wolfe, D. and Worsnop, R.: Assessing state-of-the-art capabilities for probing the
636 atmospheric boundary layer: the XPIA field campaign, Bull. Am. Meteorol. Soc.,
637 doi:10.1175/BAMS-D-15-00151.1, 2016b.

638 Mikkelsen, T.: Lidar-based research and innovation at DTU wind energy—a review, in Journal of
639 Physics: Conference Series, vol. 524, p. 12007, IOP Publishing. [online] Available from:
640 <http://iopscience.iop.org/article/10.1088/1742-6596/524/1/012007/meta> (Accessed 22 August
641 2014), 2014.

642 Mikkelsen, T., Mann, J., Courtney, M. and Sjöholm, M.: Windscanner: 3-D wind and turbulence
643 measurements from three steerable doppler lidars, in IOP Conference Series: Earth and
644 Environmental Science, vol. 1, pp. U148–U156, Institute of Physics Publishing Ltd., 2008.

645 Newman, J. F., Bonin, T. A., Klein, P. M., Wharton, S. and Newsom, R. K.: Testing and
646 validation of multi-lidar scanning strategies for wind energy applications, Wind Energy, n/a-n/a,
647 doi:10.1002/we.1978, 2016.



648 Newsom, R., Calhoun, R., Ligon, D. and Allwine, J.: Linearly organized turbulence structures
649 observed over a suburban area by dual-Doppler lidar, *Bound.-Layer Meteorol.*, 127(1), 111–130,
650 2008.

651 Newsom, R. K., Berg, L. K., Shaw, W. J. and Fischer, M. L.: Turbine-scale wind field
652 measurements using dual-Doppler lidar, *Wind Energy*, 18(2), 219–235, doi:10.1002/we.1691,
653 2015.

654 Stawiarski, C., Träumner, K., Knigge, C. and Calhoun, R.: Scopes and challenges of dual-
655 Doppler lidar wind measurements—an error analysis, *J. Atmospheric Ocean. Technol.*, 30(9),
656 2044–2062, 2013.

657 Strauch, R. G., Merritt, D. A., Moran, K. P., Earnshaw, K. B. and De Kamp, D. V.: The
658 Colorado Wind-Profiling Network, *J. Atmospheric Ocean. Technol.*, 1(1), 37–49,
659 doi:10.1175/1520-0426(1984)001<0037:TCWPN>2.0.CO;2, 1984.

660 Träumner, K., Damian, T., Stawiarski, C. and Wieser, A.: Turbulent structures and coherence in
661 the atmospheric surface layer, *Bound.-Layer Meteorol.*, 154(1), 1–25, 2015.

662 Vanderwende, B. J., Lundquist, J. K., Rhodes, M. E., Takle, E. S. and Irvin, S. L.: Observing and
663 simulating the summertime low-level jet in central Iowa, *Mon. Weather Rev.*, (2015) [online]
664 Available from: <http://journals.ametsoc.org/doi/abs/10.1175/MWR-D-14-00325.1> (Accessed 24
665 October 2015), 2015.

666 Vollmer, L., Dooren, M. van, Trabucchi, D., Schneemann, J., Steinfeld, G., Witha, B., Trujillo, J.
667 and Kühn, M.: First comparison of LES of an offshore wind turbine wake with dual-Doppler
668 lidar measurements in a German offshore wind farm, *J. Phys. Conf. Ser.*, 625(1), 12001,
669 doi:10.1088/1742-6596/625/1/012001, 2015.

670 Waldteufel, P. and Corbin, H.: On the analysis of single-Doppler radar data, *J. Appl. Meteorol.*,
671 18(4), 532–542, 1979.

672 Wang, H., Barthelmie, R. J., Clifton, A. and Pryor, S. C.: Wind Measurements from Arc Scans
673 with Doppler Wind Lidar, *J. Atmospheric Ocean. Technol.*, 32(11), 2024–2040,
674 doi:10.1175/JTECH-D-14-00059.1, 2015.

675 Wang, Y., Hocut, C. M., Hoch, S. W., Creegan, E., Fernando, H. J. S., Whiteman, C. D., Felton,
676 M. and Huynh, G.: Triple Doppler wind lidar observations during the mountain terrain
677 atmospheric modeling and observations field campaign, *J. Appl. Remote Sens.*, 10(2), 026015–
678 026015, doi:10.1117/1.JRS.10.026015, 2016.

679

680